Available online at www.sciencedirect.com
SCIENCE DIRECT
Journal of Molecular Structure 748 (2005) 77–90
Journal of MOLECULAR STRUCTURE
www.elsevier.com/locate/molstruc

Infrared spectrum and ab initio calculations of matrix isolated methanesulfonic acid species and its 1:1 water complex

A. Givan[a], A. Loewenschuss[a,*], C.J. Nielsen[b]

[a]Department of Inorganic and Analytical Chemistry, The Hebrew University of Jerusalem, Jerusalem 91904, Israel
[b]Department of Chemistry, University of Oslo, Blindern, N-0315 Oslo, Norway

Received 22 December 2004; revised 1 March 2005; accepted 1 March 2005
Available online 26 April 2005

Abstract

Vapor species of methanesulfonic acid (MSA, CH_3SO_2OH) trapped in solid Ar and Ar/H_2O matrices were investigated by FTIR spectroscopy. Intensity variations induced by matrix annealing and variations in water content indicate band assignments to monomeric and dimeric MSA species and to the 1:1 MSA·H_2O complex. Assignments are discussed in relation to MP2 and DFT calculations of vibrational frequencies. A single structure is suggested for the monomer whereas two structures of slightly different stabilization energies are suggested for both the dimer and the 1:1 MSA·H_2O complex.

Keywords: Methanesulfonic acid; FTIR spectroscopy; Matrix isolation

1. Introduction

Methanesulfonic acid (MSA, CH_3SO_2OH), along with dimethyl sulfoxide (DMSO, $(CH_3)_2SO$) and dimethyl sulfone ($DMSO_2$, $(CH3)_2SO_2$) are atmospheric oxidation products of dimethyl sulfide [1]. These species have been detected in the Antarctic troposphere [2,3], as well as in marine air, both in gas and aerosol phases and on glaciers [4].

Laboratory heterogeneous processes involving MSA may evaluate the relative contribution of MSA to marine boundary layer aerosol levels and assess the impact of these aerosols on global climate. Studies show that MSA is an oxidation product of dimethylsulfide [1], the major natural source of sulfur in the atmosphere (12–54 Tg S yr^{-1} [5]). This oxidation is accomplished by the OH (daytime prominent mechanism) and NO_3 (night) radicals [6].

It is generally accepted that the OH oxidation of dimethylsulfide occurs via two pathways: (a) hydrogen abstraction which proceeds directly to SO_2 and (b) OH addition to the sulfur atom, leading to more complex products such as MSA, DMSO and $DMSO_2$ [1].

While the gas-phase SO_2 can be oxidized directly to SO_3 and form H_2SO_4, the other products undergo more complex oxidation steps with crossing pathways [7]. Both OH abstraction and addition modes are highly dependent on temperature and O_2 partial pressure. Addition rates increase with decreasing temperature, while abstraction rates decrease. This temperature dependence explains why MSA together with dimethyl sulfoxide and dimethyl sulfone are important oxidation products in low temperature environments and hence found in measurable abundance at polar latitudes [3].

MSA, unlike dimethyl sulfone, is not a final oxidation product. Its life span is controlled by OH gas-phase concentrations. In low temperature environments it is taken up, much like other oxidation products, by aqueous surfaces. When absorbed into cloud water or icicles and in particular during aerosol formation, MSA may be oxidized by OH or H_2O_2 to sulfuric acid [8].

The ease with which a molecule can enter the gas/water interface depends on its ability to act as a center of nucleation for water molecules and form clusters. Once a critical cluster size is reached, it merges with the bulk at the interface [9]. The ability to nucleate with water molecules reflects the hydrogen-bonding ability of the molecule,

* Corresponding author. Tel.: +972 2 658 5313; fax: +972 2 658 5319.
E-mail address: loewena@chem.ch.huji.ac.il (A. Loewenschuss).

0022-2860/$ - see front matter © 2005 Elsevier B.V. All rights reserved.
doi:10.1016/j.molstruc.2005.03.015

which, in turn, depends on the nature of the S–O linkage. The S–O bonds in MSA have both covalent (double-bond) and semipolar (single-bond) characters and thus are the interaction site for hydrogen-bonding between MSA and water [10].

The infrared spectrum of MSA was previously recorded in the gas phase [11,12], and liquid [13,14] states. Also the surface molecular structure of MSA at aqueous solution surfaces was probed using vibrational sum frequency spectroscopy [15]. We found no previously recorded matrix isolation vibrational spectrum of MSA.

We have recently reported the infrared spectra of molecular sulfuric acid [16] and deuterated sulfuric acid [17] vapors, as well as of several sulfuric acid complexes (CO [18], N_2, NO, N_2O_2 [19], HCl [20], CO_2 [21]), trapped in solid argon. In all these complexes, the bonding is between one sulfuric acid OH moiety and the complexant molecule. The main spectroscopic support for this conclusion is the red shift of the OH absorption relative to its position in the free acid. However, the case for the 1:1 $H_2SO_4 \cdot H_2O$ complex [16], which plays an important role in the vapor phase nucleation of aerosols, is rather different. Although several theoretical and experimental (vapor rotational spectrum and solid thin films) studies [22–29] predict the bonding scheme mentioned above and a resulting very intense red shifted bonded OH absorption in the 3000–2800 cm^{-1} range, such line was not detected in the matrix isolated infrared spectrum [16]. On the other hand, the infrared spectrum of dimethyl sulfone (where both acidic OH moieties are replaced by the isoelectronic methyl groups)/water vapor mixtures isolated in argon [30], shows bands which were attributed to an 1:1 $(CH_3)_2SO_2 \cdot H_2O$ complex of C_s symmetry, with a single O···H bond between one of the sulfone oxygens and a water hydrogen and a secondary interaction of one S═O moiety with a methyl hydrogen.

MSA, CH_3SO_2OH, is an intermediate case between $DMSO_2$ and sulfuric acid, with one acidic OH and one methyl moiety in addition to the two S═O moieties also found in both latter molecules. It can, in principle, be attached to the H_2O complexant via both the OH and the S═O sites. The aim of the present study is, therefore, to assign vibrational spectral bands to monomeric and dimeric MSA species as well as to the 1:1 $MSA \cdot H_2O$ complex, examine the bonding schemes of these species and compare them to theoretical calculations.

2. Experimental

MSA (>99%) was supplied by Fluka, and the argon gas (99.99967%) by AGA. Water vapors were taken from deionized water, after being submitted to several degassing cycles. The argon matrix gas, either pure or premixed with water vapors in ratios ranging from 1:100 to 1:250 by standard manometric methods, was passed through a separate nozzle. The source of MSA vapors was a drop of the acid placed in a quartz tube ending in a nozzle and wrapped by a heating coil. Prior to deposition, several short degassing cycles were performed to a temperature of about 40 °C, with the deposition window, still at room temperature, turned away from the nozzle. To determine the argon/MSA ratios, MSA vapor pressures were taken from published data [31]. Nozzle temperatures were maintained in a range resulting in typical matrix/guest ratios of 1:200–1:1000 in the mixture sprayed onto a CsI window, kept at 5–18 K. Typical deposition times were 1–3 h, depending upon sample dilution, with deposition rates of argon or argon/water mixtures of several mmol h^{-1}.

Sample cooling was provided by an Air Products HS-4 Heliplex cryostat employing two HC-4 MK 1 compressor modules. Temperatures were maintained by a Lakeshore model 330 controller and Si diode sensors. Temperature cycling of the samples was conducted by slow warming ($\sim$1 K min^{-1}) up to 38–40 K, followed by fast recooling to 5 K.

Infrared spectra were recorded on a Bruker IFS 66 FTIR spectrometer, employing a DTGS detector and co-adding 32–128 scans at resolutions of 0.5–2 cm^{-1}.

3. Quantum chemical computations

MP2 and DFT calculations employing the B3LYP functional [32] were carried out using GAUSSIAN 03W [33]. The geometry of MSA, H_2O, the MSA dimer and of the 1:1 $MSA \cdot H_2O$ complexes was optimized and the vibrational frequencies, including infrared intensities were calculated. Dunning's correlation consistent aug-cc-pVTZ basis set [34–36], which includes both diffuse and polarization functions, was chosen to obtain reasonably accurate geometries of the isolated molecules and bonding of the complexes.

The calculated energy of complex formation, is the energy of the complex minus the monomer energies $\Delta E_{\text{complex}} = E(A \cdots B)^*_{ab} - E(A)_a - E(B)_b$. Here the superscript '*' refers to the geometrical structure of the complex, and the subscripts *a*, *b*, *ab* refer to the basis functions employed in the calculation of '*A*', '*B*' and '*A*···*B*', respectively. The Basis Set Superposition Error (BSSE) was assessed by the Counterpoise (CP) correction [37], $\Delta E_{\text{CP}} = E(A)^*_{ab} + E(B)^*_{ab} - E(A)^*_a - E(B)^*_b$, and the counterpoise corrected energy of complex formation is given as $\Delta E_{\text{complex}} - \Delta E_{\text{CP}}$.

3.1. Calculated frequencies of vibration

The calculated harmonic frequencies of H_2O and MSA deviate slightly from the observed fundamental transitions. A scaling of the B3LYP/aug-cc-pVTZ harmonic force field, involving two and eight parameters for H_2O and MSA,

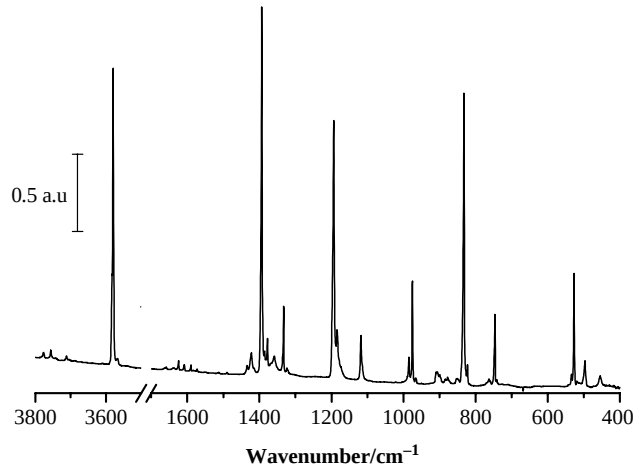

Fig. 1. Survey infrared spectrum of a 1:500 sample of MSA trapped in solid argon at 5 K.

respectively, was therefore employed to obtain an agreement between observed and calculated wavenumbers of the free molecules. The force fields were scaled according to the procedure $F_{i,j}^{\text{scaled}} = F_{i,j}^{\text{calc.}} \sqrt{\alpha_i \alpha_j}$, where α_i and α_j are scaling parameters for the valence coordinates i and j, respectively. The scaling factors derived from the observed monomer frequencies were subsequently applied to the calculated harmonic force fields of the complexes, with the scaling factors for the intermolecular 'valence' coordinates fixed to unity.

4. Spectroscopic results

4.1. Monomeric MSA

A survey infrared spectrum of MSA isolated in argon at 5 K is given in Fig. 1.

Assignment of bands to the monomeric species is, in part, based upon a comparison of their frequencies to the gas phase values [11,12] and is supported by the irreversible decrease of their intensities upon annealing. Table 1 lists the monomeric band wave number values along with the gas phase band positions as well as the analogous band frequencies of sulfuric acid and dimethyl sulfone monomers isolated in argon. The matrix shifts of the monomeric bands in the matrix relative to their gas phase values are small (<1.5%) and to the red, with the exception of the SO_2 rock, with a matrix frequency red shifted by over 4%.

The consideration of MSA as an 'intermediate case' between sulfuric acid and dimethyl sulfone is supported by the frequency values of the parallel vibrational modes, e.g. the SO_2 stretches and wag (with the SO_2 rock mode being, again, an exception).

Several low intensity sharp bands of monomeric behavior and red shifted with respect to the main bands, may be assigned to the $M^{34}SA$ isotopomeric monomers. The observed and calculated shifts are -15.9 vs. $-17.4\ \text{cm}^{-1}$, respectively, for the S═O_2 antisymmetric stretch band (similar to those found in dimethyl sulfone [30] and SO_2

Table 1
Vibration frequencies of methanesulfonic acid monomer in argon matrices (cm^{-1})

Mode	Approximate description	MSA (Ar matrix)	MSA (vapor)[a]	H_2SO_4 (Ar matrix)[b]	$DMSO_2$ (Ar matrix)[c]
ν_1	OH stretch	3582.3 (sh)[d], 3579.4	3609	3566.7	
ν_2	CH_3 antisymmetric stretch	3204.5	–	–	3023
ν_3	CH_3 antisymmetric stretch	3188.5	–	–	
ν_4	CH_3 symmetric stretch	3047.0	–	–	2942
ν_5	CH_3 antisymmetric deformation	1434.0	1418	–	1437
ν_6	CH_3 antisymmetric deformation	1422.1	1418	–	1419
ν_7	SO_2 antisymmetric stretch	1397 (sh)[d], 1393.4, 1377.4[e]	1403	1452.4	1340.1
ν_8	CH_3 symmetric deform.	1332.8	1336	–	–
ν_9	SO_2 symmetric stretch	1199 (sh)[d], 1193.6	1202	1216.1	1157.2
ν_{10}	SOH bend	1118.3	1122	1156.9(as), 1135.9 (s)	–
ν_{11}	CH_3 rock	975.3	980	–	931.6
ν_{12}	CH_3 rock	967.0	980	–	–
ν_{13}	SO stretch	835.5 (sh)[d], 832.5, 822.4[e]	828	881.7 (as), 831.4 (s)	–
ν_{14}	CS stretch	746.5, 741.7[e]	748	–	747.2 (as), 687.8 (s)
ν_{15}	SO_2 deformation	526.9	528	558 (rock)	
ν_{16}	SO_2 wag	496.8	502	548 (bend)	493.6 (bend)
ν_{17}	SO_2 rock	454.4	473	505.7 (wag)	461.3 (wag)
ν_{18}	SO_2 twist			421.7 (O–S═O) twist	–
ν_{19}	CSO bend			378.5 (O–S═O) bend	–
ν_{20}	CH_3 torsion	–			–
ν_{21}	OH torsion	–		287.7 (as), 224 (s)	–

[a] Refs. [11,12].
[b] Ref. [16].
[c] Ref. [30].
[d] Unstable site.
[e] (^{34}S) isotopomer, for calculated shifts, see text.

[38] monomers in solid argon), −10.1 vs. −10.4 cm^{-1}, respectively, for the S–O stretch and −4.8 vs. −4.6 cm^{-1}, respectively, for the C–S stretch.

Blue shifted shoulders are observed on the most prominent monomeric bands (Table 1). Relative to the main absorptions, their intensities strongly depend upon deposition conditions and are significantly and irreversibly reduced upon annealing (Fig. 2a–d). They are, therefore, attributed to MSA monomers trapped in unstable sites in the argon matrix.

Table 2 lists the results of DFT calculations of monomeric MSA vibrational band frequencies and intensities and compares them with the observed values. The deviations of the calculated frequencies from the observed values are very small (less than 1.3% for the CH stretches) with the exception of the 454.4 cm^{-1} SO_2 wag (~2.4%). The monomer structure resulting from the above mentioned calculations is shown in Fig. 3.

4.2. The dimer $(MSA)_2$ and the 1:1 $MSA \cdot H_2O$ complex

The prominent monomeric absorptions are often accompanied by additional bands, enhanced by temperature cycling, which may be assigned to dimeric and higher polymeric MSA species as well as to water containing MSA species.

The fraction of dimeric species in MSA vapors can be calculated from:

$$(4K_p p_{tot} + 1)x^2 - (4K_p p_{tot} + 1)x + K_p p_{tot} = 0$$

where x is the dimer fraction in the vapor and results in $<1\%$ at typical deposition temperatures. $K_p(T)$ was calculated from the DFT results. The temperature dependence of x, based on the vapor pressure data of Tang and Munkelwitz [31], is shown in Fig. 4. The small amount of dimer existing in the vapor increases during the matrix relaxation in

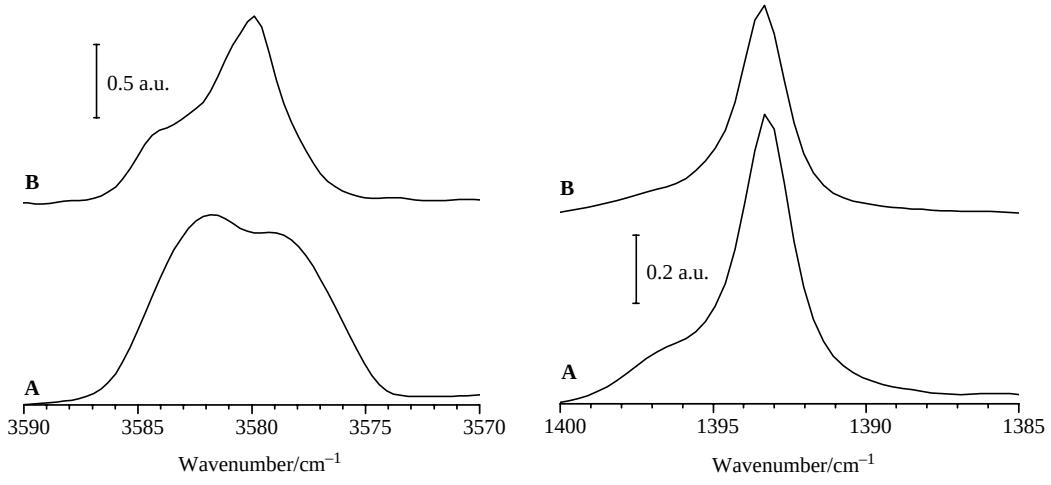

(a) The OH stretch mode

(b) The SO_2 antisymmetric stretch mode

(c) The SO_2 symmetric stretch mode

(d) The SO stretch mode

Fig. 2. Site effects in monomeric absorption bands of argon isolated MSA. For all spectra: (A) as deposited at 5 K. (B) After temperature cycling to 24 K.

Table 2
Calculated and observed fundamental vibration modes (/cm^{-1}) and infrared band intensities (/km mol^{-1}) in water and methanesulfonic acid

Mode	Approximate description	Calculated[a]	I_{IR}	Scaled[b]	I_{IR}	Observed[c]	Δ
$\nu_1(A_1)$	OH symmetric stretch	3796.2	4.6	3637.7	4.6	3638.0	0.3
$\nu_2(A_1)$	HOH bend	1627.0	75.8	1590.0	75.8	1590.0	0.0
$\nu_3(B_2)$	OH antisymmetric stretch	3898.9	63.0	3736.0	63.0	3735.7	−0.3
ν_1	OH stretch	3761.5	125.4	3579.4	125.5	3579.4	0.0
ν_2	CH_3 antisymmetric stretch	3172.2	0.1	3185.3	0.1	3204.5	19.3
ν_3	CH_3 antisymmetric stretch	3163.0	0.2	3176.1	0.2	3188.5	12.4
ν_4	CH_3 symmetric stretch	3067.1	0.1	3079.8	0.1	3047.0	−32.8
ν_5	CH_3 antisymmetric deformation	1458.8	0.7	1431.8	8.3	1434.0	2.2
ν_6	CH_3 antisymmetric deformation	1457.3	5.0	1427.8	4.9	1422.1	−5.7
ν_7	SO_2 antisymmetric stretch	1370.3	269.2	1394.0	262.4	1393.4	−0.6
ν_8	CH_3 symmetric deformation	1353.3	11.4	1327.3	15.7	1332.8	5.5
ν_9	SO_2 symmetric stretch	1175.3	207.4	1194.2	198.0	1193.6	−0.6
ν_{10}	SOH bend	1121.2	26.8	1118.5	28.5	1118.3	−0.2
ν_{11}	CH_3 rock	990.0	25.8	979.7	41.0	975.3	−4.4
ν_{12}	CH_3 rock	979.0	1.9	966.3	2.0	967.0	0.7
ν_{13}	SO stretch	793.4	204.0	833.0	193.2	832.5	−0.5
ν_{14}	CS stretch	707.9	37.8	745.6	35.5	746.5	0.9
ν_{15}	SO_2 deformation	501.2	40.8	528.8	41.1	526.9	−1.9
ν_{16}	SO_2 wag	475.3	17.9	499.4	17.7	496.8	−2.6
ν_{17}	SO_2 rock	421.0	14.1	440.9	13.9	454.4	13.5
ν_{18}	SO_2 twist	318.9	16.4	332.7	10.9	336.0[d]	3.3
ν_{19}	CSO bend	305.9	10.3	319.6	11.8	326.0[d]	6.4
ν_{20}	CH_3 torsion	212.3	26.0	214.1	32.4		
ν_{21}	OH torsion	190.0	37.2	192.0	35.2		

[a] Results from B3LYP/aug-cc-pVTZ calculations.
[b] See text for scaling procedure. Scaling factors for H_2O: OH, 0.918; HOH, 0.955. Scaling factors for MSA: OH, 0.906; CH, 1.008; SCH/HCH, 0.96; S═O, 1.042; SOH, 0.976; S–O, 1.107; SC, 1.119; OSO/OSC, 1.111; OSCH/CSOH, 1.0 (fixed).
[c] This work except where noted.
[d] From Raman spectra of the liquid, Ref. [14].

the process of deposition and then increases further in our annealing experiments.

The dimer may assume two forms, of C_i and C_2 symmetries, respectively. The calculated structures of the C_i and C_2 forms of MSA dimers are shown in Fig. 5. At 320 K, the amount of the former is predicted by the DFT calculations, to be approximately 10 times that of the latter. A further discussion of the energetics of the dimer in its two forms is given below. Calculated vibrational frequencies of both possible dimeric species are listed in Table 3 along with the relevant observed values for the assigned dimer bands.

Water containing MSA species are distinguished by their enhancement with increasing water vapor content of the deposited mixture. Water and sulfuric acid remnants (identified by its prominent infrared OH stretch at 3566.7 cm^{-1}) are always found in the deposited MSA

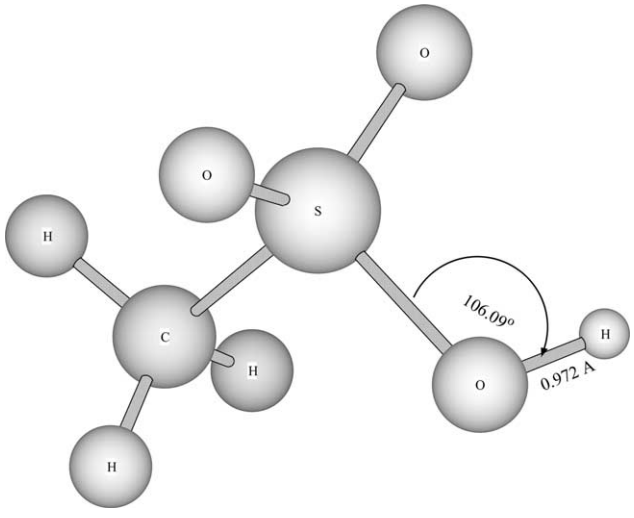

Fig. 3. Calculated structure of the MSA monomer.

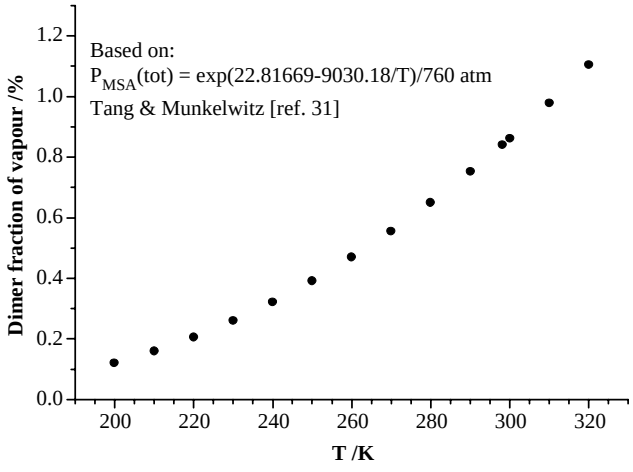

Fig. 4. Fraction of dimeric species in MSA vapor for experimental deposition temperatures.

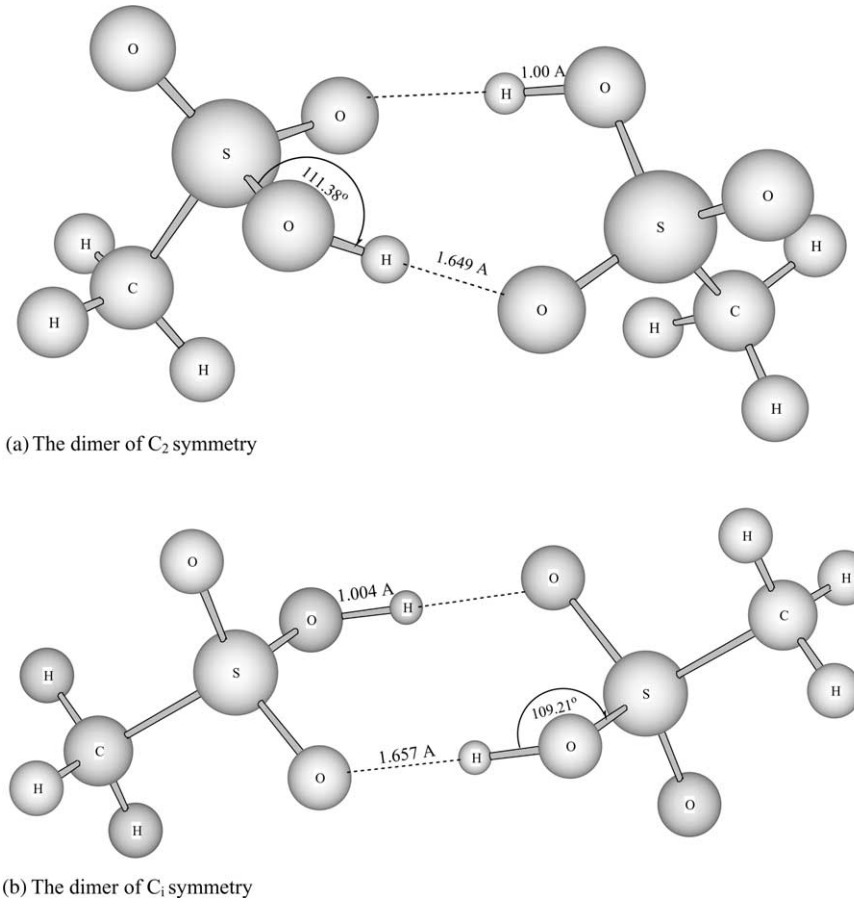

(a) The dimer of C_2 symmetry

(b) The dimer of C_i symmetry

Fig. 5. Calculated structures of the MSA dimer. (a) C_i form. (b) C_2 form.

samples. As water molecules are the species of highest mobility in the matrices, their effects are always observed in annealing experiments. Table 4 lists the frequencies assigned to the MSA·H_2O complex along with calculated values for two possible structures 1:1 shown in Fig. 6.

In the following text, results for both the dimeric and water containing species, will be described separately for each of the relevant vibrational mode. Temperature cycling experiments are shown in Fig. 7a–i and water concentration effects in Fig. 8a–i.

4.3. The OH stretch region

Figs. 7 and 8 show the OH stretch region of matrix isolated MSA. The spectrum trace of Fig. 7a, trace A, of an 500:1 argon/MSA is of a sample deposited at 5 K, containing only residual water concentrations. It shows bands assigned to the OH stretch of the MSA monomer, trapped in its two sites, at 3579.4 and 3582.3 cm^{-1}, respectively, together with a weak absorption of the antisymmetric OH stretch of sulfuric acid at 3566.8 cm^{-1} [16]. Bands of antisymmetric and symmetric OH stretches of H_2O monomers and polymers [39–54] are also recorded and are seen to be enhanced both by annealing (Fig. 7a, trace B) and with increasing water content of the matrix (Fig. 8a, traces A, B, C).

Two additional bands of very weak and weak intensity, respectively, are found at 3687.2 and 3539.2 cm^{-1}. They also gain intensity during annealing (Fig. 7a, trace B) and with increasing water concentration in the matrix (Fig. 8a, traces B, C) and should, therefore, be assigned to water containing species. According to calculations (Tables 3 and 4), the MSA moieties of neither the more stable MSA dimer nor the 1:1 MSA·H_2O complex, have vibrational modes in this frequency region. On the other hand, these two absorptions resemble both in position and relative intensities the free and bonded OH stretches of the water dimer at 3707 and 3574 cm^{-1}, respectively [46–54]. The lower frequency band (at 3539.2 cm^{-1}) is also close to the position of the bonded OH stretch absorption of the H_2O moiety in the $DMSO_2$·H_2O complex at 3568 cm^{-1}, recently reported by us [30]. We, therefore, assign the 3687.2 cm^{-1} and the 3539.2 cm^{-1} bands to the free and bonded OH, respectively, of the H_2O moiety in the 1:1 MSA·H_2O complex. Theoretical calculations indicate two possible structures for the complex (Fig. 6) and the comparison of observed and calculated values (Table 5) 3694.1 and 3500.1 cm^{-1}, respectively, indicate

Table 3
Observed and calculated[a] fundamental modes of vibration (/cm^{-1}) and infrared band intensities (/km mol^{-1}) of the methanesulfonic acid dimer.

Approximate mode description	C_2 form			C_2 form			Observed (this work)	Liquid (Ref. [15])
	Mode no.	Calculated[b]	I_{IR}	Mode no.	Calculated[b]	I_{IR}		
CH_3 antisymmetric stretch	ν_{26}(B)	3182.9	0.2	$\nu_1(A_g)$	3181.3			
CH_3 antisymmetric stretch	ν_1(A)	3182.8	0.0	$\nu_{25}(A_u)$	3181.3	0.3		
CH_3 antisymmetric stretch	ν_2(A)	3177.0	0.3	$\nu_2(A_g)$	3175.1			
CH_3 antisymmetric stretch	ν_{27}(B)	3176.9	0.1	$\nu_{26}(A_u)$	3175.1	0.5	3172.0	
CH_3 symmetric stretch	ν_{28}(B)	3079.1	1.1	$\nu_{27}(A_u)$	3077.4	15.0		
CH_3 symmetric stretch	ν_3(A)	3079.1	0.1	$\nu_3(A_g)$	3077.2			
OH stretch	ν_{29}(B)	3025.7	3439.1	$\nu_{28}(A_u)$	3047.4	3275.7	3030.0	3000
OH stretch	ν_4(A)	2945.9	29.6	$\nu_4(A_g)$	2970.1			
CH_3 antisymmetric deformation	ν_5(A)	1432.5	4.0	$\nu_5(A_g)$	1433.5			
CH_3 antisymmetric deformation	ν_{30}(B)	1430.5	1.4	$\nu_{29}(A_u)$	1429.9	5.1		
CH_3 antisymmetric deformation	ν_{31}(B)	1428.2	8.9	$\nu_6(A_g)$	1428.1		1426.8	1418
CH_3 antisymmetric deformation	ν_6(A)	1428.1	0.4	$\nu_{30}(A_u)$	1427.5	7.7		
SO_2 antisymmetric stretch	ν_7(A)	1386.1	150.2	$\nu_7(A_g)$	1390.4		1385.7	
SO_2 antisymmetric stretch	ν_{32}(B)	1365.6	546.3	$\nu_{31}(A_u)$	1368.7	744.6	1367.9	1343
CH_3 symmetric deformation	ν_8(A)	1330.0	16.5	$\nu_8(A_g)$	1330.0			
CH_3 symmetric deformation	ν_{33}(B)	1328.2	40.3	$\nu_{32}(A_u)$	1329.5	39.2	1323.4	1333
S–O–H bend	ν_9(A)	1275.0	10.6	$\nu_9(A_g)$	1280.1			1174
S–O–H bend	ν_{34}(B)	1255.5	151.2	$\nu_{33}(A_u)$	1264.2	134.6		
SO_2 symmetric stretch	ν_{35}(B)	1173.2	352.7	$\nu_{34}(A_u)$	1179.3	373.5	1184.1, 1178.5	1150
SO_2 symmetric stretch	ν_{10}(A)	1120.4	27.3	$\nu_{10}(A_g)$	1124.4			
CH_3 antisymmetric deformation	ν_{11}(A)	991.0	44.6	$\nu_{35}(A_u)$	989.7	170.6	985.1, 990	987
CH_3 antisymmetric deformation	ν_{36}(B)	989.2	134.1	$\nu_{11}(A_g)$	987.4			
CH_3 antisymmetric deformation	ν_{12}(A)	972.6	1.9	$\nu_{12}(A_g)$	970.8			
CH_3 antisymmetric deformation	ν_{37}(B)	970.9	0.9	$\nu_{36}(A_u)$	969.9	3.3		
S–O stretch	ν_{13}(A)	908.3	93.3	$\nu_{37}(A_u)$	908.4	251.6	909.6, 906.4	900
S–O stretch	ν_{38}(B)	907.6	163.7	$\nu_{13}(A_g)$	901.3			
O–H torsion	ν_{14}(A)	815.8	54.7	$\nu_{38}(A_u)$	787.0	125.5		
O–H torsion/C–S stretch[c]	ν_{39}(B)	780.5	7.3	$\nu_{14}(A_g)$	772.7		769.5	771
C–S stretch	ν_{15}(A)	769.5	20.2	$\nu_{39}(A_u)$	765.2	24.6	759.0	670
O–H torsion/ C–S stretch[c]	ν_{40}(B)	754.3	51.7	$\nu_{15}(A_g)$	756.8			
O═S═O rock	ν_{16}(A)	537.3	51.6	$\nu_{40}(A_u)$	540.1	53.1	542.0	534
O═S═O rock	ν_{41}(B)	530.8	47.7	$\nu_{16}(A_g)$	533.7			
O═S═O bend	ν_{42}(B)	514.1	66.1	$\nu_{41}(A_u)$	520.1	96.6	519.0	501
O═S═O bend	ν_{17}(A)	510.1	1.8	$\nu_{17}(A_g)$	513.1			
O═S═O twist	ν_{43}(B)	491.7	7.2	$\nu_{42}(A_u)$	492.0	6.8	501.9	480
O═S═O twist	ν_{18}(A)	469.0	3.9	$\nu_{18}(A_g)$	470.4			
O═S═O wag	ν_{19}(A)	348.7	0.7	$\nu_{19}(A_g)$	337.8			
O═S═O wag	ν_{44}(B)	338.3	2.2	$\nu_{43}(A_u)$	328.9	1.0		
C–S–O bend	ν_{45}(B)	312.5	2.7	$\nu_{20}(A_g)$	312.3			
C–S–O bend	ν_{20}(A)	309.5	0.2	$\nu_{44}(A_u)$	311.2	1.9		
CH_3 torsion	ν_{46}(B)	222.6	20.4	$\nu_{45}(A_u)$	219.2	16.7		
CH_3 torsion	ν_{21}(A)	210.1	0.2	$\nu_{21}(A_g)$	212.0			
Intermolecular	ν_{47}(B)	186.5	21.3	$\nu_{46}(A_u)$	181.7	32.3		
Intermolecular	ν_{22}(A)	136.5	0.1	$\nu_{22}(A_g)$	153.1			

(*continued on next page*)

Table 3 (*continued*)

Approximate mode description	C_2 form			C_2 form			Observed (this work)	Liquid (Ref. [15])
	Mode no.	Calculated[b]	I_{IR}	Mode no.	Calculated[b]	I_{IR}		
Intermolecular	$\nu_{23}(A)$	135.8	1.0	$\nu_{23}(A_g)$	130.5			
Intermolecular	$\nu_{24}(A)$	48.7	1.2	$\nu_{24}(A_g)$	38.3			
Intermolecular	$\nu_{48}(B)$	33.3	9.5	$\nu_{47}(A_u)$	27.1	10.7		
Intermolecular	$\nu_{25}(A)$	25.3	0.0	$\nu_{48}(A_u)$	22.0	7.5		

[a] Results from B3LYP/aug-cc-pVTZ.
[b] The scaling factors (included as a footnote in Table 2) were applied to the calculated harmonic force fields of the complexes. Scaling factors for the intermolecular valence coordinates were constrained to unity. See text for details on the scaling procedure.
[c] Significant mode mixing. Order of dominance-C_2 form: OH,CS; C_i form: CS,OH.

a better similarity to structure I, which according to calculations is, indeed, the more stable form (Table 5).

Similar to the 1:1 MSA·H_2O complex, also for the MSA dimer, two structural forms of C_i and C_2 symmetry, respectively, are possible (Fig. 5). The absence, in this region, of any bands with dimeric MSA character (i.e. bands enhanced with concentration and temperature cycling, but not with increasing water content of the matrix), which could be assigned to a free OH stretch of the C_2 form of the dimer, is in line with the theoretical prediction (Table 5) of cyclic structures for both dimer forms.

4.4. The 2800–3300 cm^{-1} (C–H stretch) region

This spectral region is dominated by the 3204.5 and 3188.5 cm^{-1} C–H stretch bands of monomeric MSA. Two additional lines, moderately increased upon annealing (Fig. 7b), the 3172.0 cm^{-1} shoulder and the broad band centered at 3030.0 cm^{-1} do not grow when the sample water concentration is increased (Fig. 8b). Accordingly, we associate these bands with the more stable C_i form of the MSA dimer. The weak band at 3172.0 cm^{-1} is assigned to the antisymmetric C–H stretch (calculated at 3175.1 cm^{-1}, Table 3) and the 3030.0 cm^{-1} to the O–H stretch (calculated at 3047.4 cm^{-1}, Table 3).

A very wide absorption, peaking at 2870 cm^{-1} with a shoulder at 2930 cm^{-1}, is significantly enhanced upon annealing (Fig. 7b). Raising the water concentration of the sample increases the total absorption intensity, with the latter feature showing the greater enhancement. The 2930 cm^{-1} feature may, then, be associated with the 1:1 MSA·H_2O complex and is attributed to its the bonded O–H stretch of MSA (calculated 3009.7 cm^{-1}, Table 4). An analogous broad band, similarly red shifted from the free acid OH stretch frequency, recorded in the infrared spectrum of the 1:1 HNO_3·H_2O complex [55–58], was assigned to the OH stretch of the HNO_3 moiety.

4.5. H_2O bending mode region

The absorptions in this region (Figs. 7c and 8c) belong almost exclusively to monomeric and polymeric H_2O species [39–54]. A single extra, very weak band is found at 1600 cm^{-1} and is observed to slightly enhance upon annealing.

Higher water ratios in the matrix (Fig. 8c) increase the concentrations of the polymeric water species in the sample. The very weak 1600.0 cm^{-1} feature becomes masked by the growing in of the 1601.8 cm^{-1} $(H_2O)_3$ absorption. We assign this 1600.0 cm^{-1} band to the bending mode of the H_2O moiety of the 1:1 MSA·H_2O complex, with a very similar calculated frequency at 1603.3 cm^{-1} (Table 4).

Table 4
Calculated and observed fundamental modes of vibration (/cm^{-1}) and infrared band intensities (/km mol^{-1}) of the 1:1 MSA·H_2O methanesulfonic acid water complex

Mode	Approximate mode description	Complex I		Complex II		Observed	Δ = Obs. − I
		Calculated[a]	I_{IR}	Calculated[a]	I_{IR}		
ν_1	Free OH stretch in water	3694.1	108.1	3701.6	102.0	3687.2	−6.9
ν_2	Bonded OH stretch in water	3500.1	204.8	3519.6	166.3	3539.2	39.1
ν_3	CH_3 antisymmetric stretch	3182.2	0.2	3182.1	0.5		
ν_4	CH_3 antisymmetric stretch	3174.9	0.1	3173.4	0.6		
ν_5	CH_3 symmetric stretch	3078.0	0.2	3078.1	4.2		
ν_6	Bonded OH stretch in MSA	3009.7	1102.4	3071.4	995.9	2930.0	−79.7
ν_7	HOH bend in water	1603.3	59.8	1592.3	45.8	1600.0	−3.3
ν_8	CH_3 antisymmetric deformation	1437.3	49.9	1434.8	25.3		
ν_9	CH_3 antisymmetric deformation	1427.9	3.8	1427.9	3.3	1426.8	−1.1
ν_{10}	S–O–H bend	1410.8	180.2	1402.0	257.3	1334.0	−76.8
ν_{11}	CH_3 symmetric deformation	1330.3	58.3	1326.7	23.6		
ν_{12}	SO_2 antisymmetric stretch	1316.5	99.6	1303.2	103.3	1304.0	−12.5
ν_{13}	SO_2 symmetric stretch	1162.9	156.3	1164.6	148.2	1173.1	10.2
ν_{14}	CH_3 rock	983.3	63.4	981.0	64.4	979.7	−3.6
ν_{15}	CH_3 rock	968.2	2.0	965.8	1.4		
ν_{16}	SO stretch	883.1	156.1	880.6	155.2	884.1	1.0
ν_{17}	OH torsion in MSA	839.4	89.8	810.1	75.4	877.2	37.8
ν_{18}	CS stretch	762.9	20.5	761.5	24.2	761.3	−1.6
ν_{19}	Intermolecular (OH)	597.7	207.7	571.9	233.8		
ν_{20}	OSO bend	535.0	43.5	534.7	38.1	534.2	−0.8
ν_{21}	OSO/intermolecular	516.3	23.3	513.0	30.4	513.7	−2.6
ν_{22}	OSO bend	476.7	15.8	481.9	14.9		
ν_{23}	intermolecular	366.6	84.9	339.5	15.3		
ν_{24}	OSO bend	338.9	0.9	327.1	30.0		
ν_{25}	OSO bend	308.6	9.9	306.1	12.4		
ν_{26}	Intermolecular	282.4	99.5	265.4	110.7		
ν_{27}	Intermolecular	231.0	26.9	221.6	24.3		
ν_{28}	CH_3 torsion	202.7	0.7	203.3	1.3		
ν_{29}	Intermolecular	154.7	17.8	148.8	19.9		
ν_{30}	Intermolecular	37.8	8.4	47.8	1.6		

[a] The scaling factors (included as a footnote in Table 2) were applied to the calculated harmonic force fields of the complexes. Scaling factors for the intermolecular valence coordinates were constrained to unity. See text for details on the scaling procedure.

4.6. The CH_3 antisymmetric deformation region

The monomeric CH_3 antisymmetric deformation bands are found at 1434.0 cm^{-1} and 1422.1 cm^{-1}. A single additional band appears at 1426.8 cm^{-1}. It not only clearly grows during annealing (Fig. 7d), but its intensity is also enhanced when the water content of the matrix is raised (Fig. 8d). This behavior would indicate its assignment to the 1:1 MSA·H_2O complex, calculated at 1427.9 cm^{-1} (Table 4). However the dimer of C_i form has the calculated frequency for the analogous mode at a very similar value, 1428.1 cm^{-1}. We are thus led to assign the observed 1426.8 cm^{-1} band to both the 1:1 MSA·H_2O complex and the C_i MSA dimer.

4.7. The SO_2 antisymmetric stretch and CH_3 symmetric deformation region

This spectral region is dominated by the SO_2 antisymmetric stretch band at 1393.4 cm^{-1} (calculated value 1394.0 cm^{-1}, Table 2) flanked by the unstable site band at 1397 cm^{-1} at higher frequencies (Fig. 2b) and by the $^{34}SO_2$ isotopomer band at 1377.4 cm^{-1}, on its low frequency side. The second intense monomeric band in this range is the CH_3 symmetric deformation at 1332.8 cm^{-1} (calculated value 1327.3 cm^{-1}, Table 2).

Additional bands, weaker but gaining intensity only upon annealing, are observed at 1385.8, 1368.2, 1358.8, 1334.0 cm^{-1} (a shoulder on the 1332.8 cm^{-1} band), 1323.4 and 1304.0 cm^{-1}. Of these, only the 1334.0 and 1304.0 cm^{-1} band intensities grow when the sample water concentration is increased (Fig. 8d) and lead to the attribution of these bands to the 1:1 MSA·H_2O complex: the 1304.0 cm^{-1} broad band is assigned to its SO_2 antisymmetric stretch (calculated value 1316.5 cm^{-1}, Table 4), and the line at 1334.0 cm^{-1} is ascribed to its SOH bending mode. The calculated value for the latter is 1410.8 cm^{-1} (Table 4) and we note the significant deviation of the calculated value from the observed band position, characteristic of modes involving the hydroxyl hydrogen.

The other non-monomeric bands can be associated with the dimeric MSA species. The 1367.9 cm^{-1} band is assigned to the SO_2 antisymmetric stretch of the C_i dimer

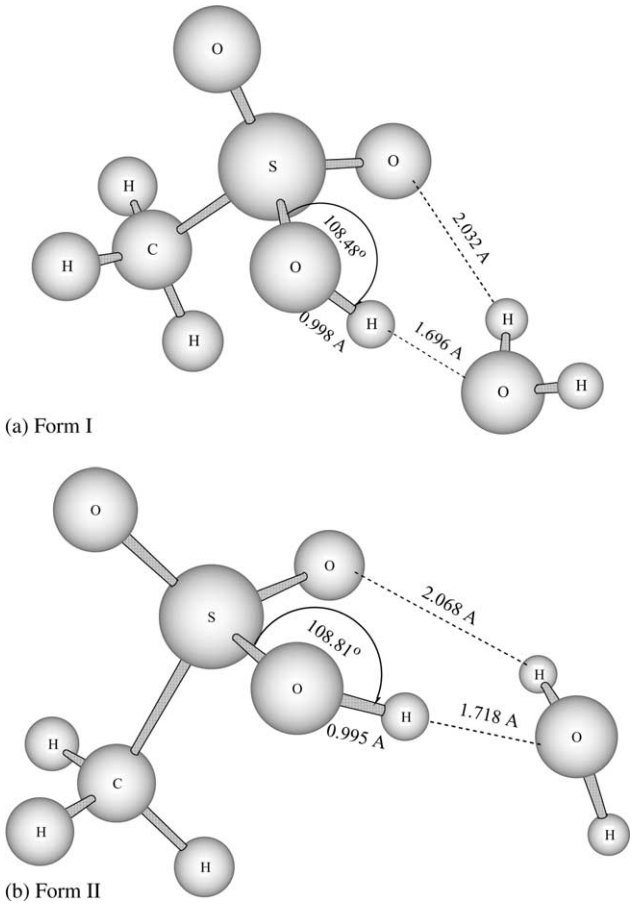

Fig. 6. Calculated structures of the MSA·H_2O complex. (a) MSA·H_2O_I. (b) MSA·H_2O_{II}.

(calculated at 1368.7 cm^{-1}, Table 3) and the 1323.4 cm^{-1} to its CH_3 deformation (calculated at 1329.5 cm^{-1}, Table 3).

The remaining 1385.8 and 1358.8 cm^{-1} bands are very close in position to the calculated frequencies of the MSA dimer in its C_2 form (1386.1 and 1365.6 cm^{-1}, respectively, Table 3). However, their intensity relative to the bands of the C_i form, is excessive when their expected abundance is taken into consideration.

4.8. The SO_2 symmetric stretch and SOH bend region

The monomeric bands in this region are the 1193.6 cm^{-1} SO_2 symmetric stretch and the 1118.3 cm^{-1} SOH bend. Three additional peaks are observed–the strong 1184.1 cm^{-1} band, the weak 1178.5 cm^{-1} band, which appears during annealing and the 1173.1 cm^{-1}. All three bands grow during annealing (Fig. 7e), but the 1173.1 cm^{-1} band also shows clear dependence upon water concentration in the matrix (Fig. 8e).

The 1184.1 cm^{-1} band is assigned to the C_i MSA dimer (calculated at 1179.3 cm^{-1}, Table 3), and the 1173.1 cm^{-1} band to the 1:1 MSA·H_2O complex (calculated at 1162.9 cm^{-1}, Table 4). The weak 1178.5 cm^{-1} peak may, again, be attributed to traces of the C_2 dimer (calculated at 1173.2 cm^{-1}, Table 3) or to a higher MSA polymer.

4.9. The CH_3 antisymmetric deformation region

In addition to the two monomeric lines at 975.3 and 967.0 cm^{-1} (Table 1), three more bands are observed in this region. The strong band 985.1 cm^{-1} is clearly present in the spectrum trace of the sample as deposited at 5 K and significantly enhanced upon annealing (Fig. 7f). Two much weaker bands appear upon annealing at 979.7 and 990.0 cm^{-1}. Of these, the former (979.7 cm^{-1}) increases with increasing water concentration in the matrix (Fig. 8f).

The strong 985.1 cm^{-1} band is attributed to the MSA C_i dimer (calculated at 989.7 cm^{-1}, Table 3) and the water concentration dependent 979.7 cm^{-1} band to the 1:1 MSA·H_2O complex (calculated at 983.3 cm^{-1}, Table 4). The weak and broad 990.0 cm^{-1} feature may be attributed to the C_2 dimer calculated at 989.2 cm^{-1} (Table 3).

4.10. S–O stretch region

The monomeric bands in this region are the S–O stretch at 832.5 cm^{-1} with its ^{34}S counterpart at 822.4 cm^{-1} at lower frequencies and the unstable site band at 835.5 cm^{-1} to higher frequencies.

The slightly split feature at 909.6 and 906.4 cm^{-1}, with intensity growing upon annealing (Fig. 7f), is assigned to the C_i MSA dimer (calculated value 908.4 cm^{-1}, Table 3).

Additional bands, increasing in intensity with the water concentration in the matrix (Fig. 8f) were recorded at 884.1 and the 877.2 cm^{-1} are assigned to the 1:1 MSA·H_2O complex. Calculations place the S–O stretch at 883.1 cm^{-1} and the OH torsion at 839.4 cm^{-1} (Table 4). Accordingly, the 884.1 cm^{-1} is assigned to the S–O stretch and the 877.2 cm^{-1} band to the OH torsion of the 1:1 MSA·H_2O complex.

The very weak 899.4 cm^{-1} band remains unassigned.

4.11. S–C stretch

The monomer band in this region is located at 746.5 cm^{-1} and has an ^{34}S isotopomeric satellite at 741.7 cm^{-1}. The non-monomeric band with water concentration dependent intensity is observed at 761.3 cm^{-1} (Fig. 8g). The assignment of this band to the 1:1 MSA·H_2O complex is supported by the calculated value of 762.9 cm^{-1} (Table 4).

Two absorptions with dimeric characteristics, enhanced upon annealing but independent of water concentration, were recorded at 769.5 and 759.0 cm^{-1} (Fig. 7g). The calculations for the C_i dimer indicate strong mixing of the S–C stretch and the OH torsions, with calculated values at 765.2 and 787.0 cm^{-1} (Table 3).

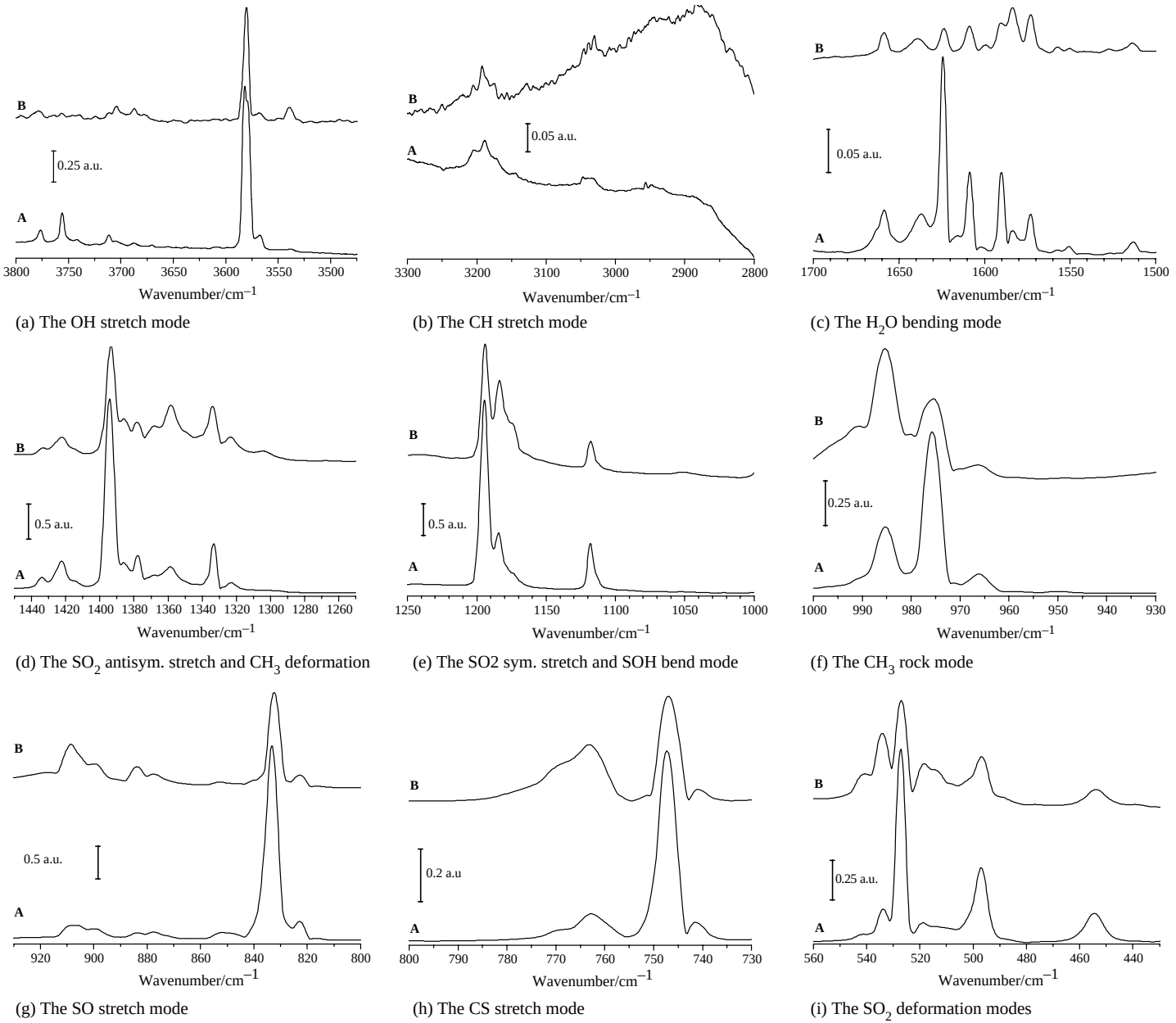

Fig. 7. Annealing effect. For all spectra: (A) as deposited at 5 K. (B) After temperature cycling to 24 K.

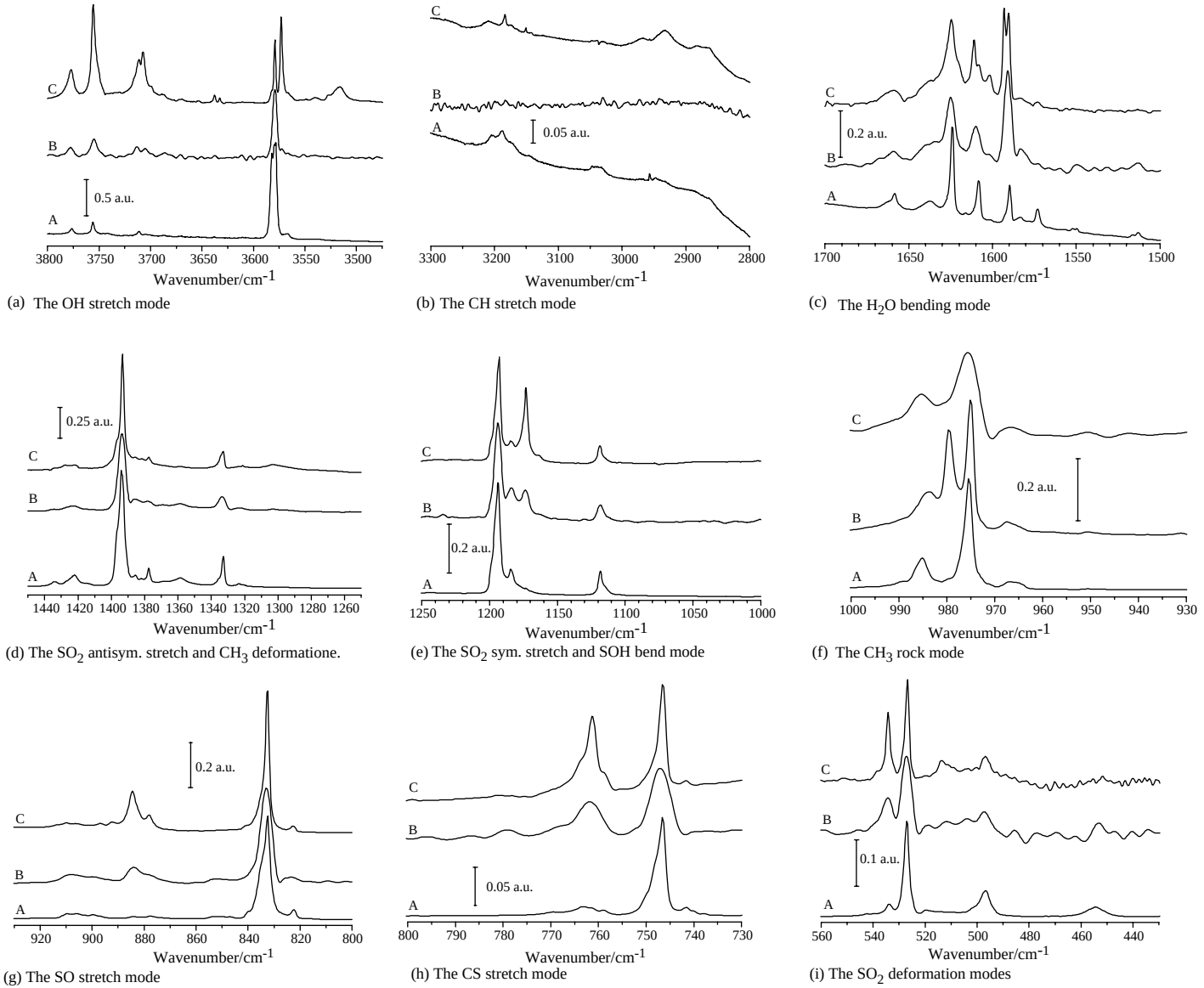

Fig. 8. Water concentration effect. For all spectra: (A) MSA in solid Ar with residual water traces. (B) MSA in an Ar/water = 500:1 matrix. (C) MSA in an Ar/water = 70:1 matrix.

Table 5
Calculated (B3LYP/aug-cc-pVTZ) electronic energies, enthalpies and Gibbs free energies of formation of complexes involving water and methanesulfonic acid (/kJ mol^{-1})

Complex	$\Delta_f E_{electronic}$[a]	$\Delta_f H_{298.15}$	$\Delta_f H_{30}$	$\Delta_f G_{298.15}$	$\Delta_f G_{30}$
$H_2O \cdot H_2O$	−18.9 (−0.2)	−12.1	−11.0	13.6	−9.2
$MSA \cdot H_2O_I$	−43.4 (−0.7)	−35.9	−33.2	4.3	−30.3
$MSA \cdot H_2O_{II}$	−39.7 (−0.7)	−32.5	−30.3	7.4	−27.0
$MSA \cdot MSA_{C_i}$	−66.8 (−1.9)	−61.6	−61.3	−15.8	−56.9
$MSA \cdot MSA_{C_2}$	−64.6 (−1.7)	−59.6	−59.2	−10.6	−54.5

[a] The Counterpoise correction, given in parenthesis, is included in the electronic energy.

4.12. SO_2 deformations

Three monomeric bands were located in this region—the 526.9 cm^{-1} SO_2 bend, the 496.8 cm^{-1} SO_2 wag and the 454.4 cm^{-1} SO_2 rock. In addition, two bands at 534.2 and 513.7 cm^{-1} show water concentration dependence (Fig. 8i). The corresponding calculated frequencies for the 1:1 $MSA \cdot H_2O$ complex are 535.0 and 516.3 cm^{-1}, respectively (Table 4).

Three dimeric bands, with intensity increasing during annealing (Fig. 7i) but not sensitive to water concentration were recorded at 542.0, 519.0 and 501.9 cm^{-1}. The corresponding calculated values for the C_i dimer are 540.1 cm^{-1} for the SO_2 bend mode, 520.1 cm^{-1} for the SO_2 rock mode and 492.0 cm^{-1} for the SO_2 twist (Table 3).

5. Structure of the complexes and their energies of formation

A scan of the potential surface of the 1:1 $MSA \cdot H_2O$ complex produced two minimum energy structures, denoted I and II as illustrated in Fig. 6A. The energy difference between the lower energy conformer, I, and the high energy conformer, II, is only 3.6 kJ mol^{-1} with a low barrier of about 1.1 kJ mol^{-1} between them. Annealing to 20 K, our procedure to distinguish the non-monomeric bands, ensures complete conversion to the low energy form I on a seconds time scale. The pivotal structure parameters as well as the changes relative to the free molecules are included in Fig. 6A. The calculated enthalpy and Gibbs free energy change upon complex formation of conformer I at 298.15 K is −35.9 and 7.4 kJ mol^{-1}, respectively (Table 5). With a positive Gibbs free energy, complex formation between MSA and water will not take place to any significant extent under normal conditions at room temperature. However, at matrix deposition temperatures, the formation of the complex is thermodynamically favored. It is kinetically enhanced by the annealing process which facilitates the mobility of the trapped molecules and, in particular of the lighter H_2O molecules, through matrix imperfection to interaction distances.

It may be argued that although DFT hybrid methods, like B3LYP, are quite reliable in estimating bonding energies of complexes they do not include the dispersion interactions. These can be quite large for weakly dipolar bonded complexes. We therefore also calculated the binding energy of the MSA C_i-dimer at the MP2/aug-cc-pVTZ level. The BSSE corrected energy of complexation is −77 kJ mol^{-1} compared to the B3LYP value of −66 kJ mol^{-1}. Thus, a naïve estimate of the dispersion interaction in the dimmer would be ca. 10 kJ mol^{-1}. However, the BSSE is −11 kJ mol^{-1} and much larger basis set calculations are obviously required to get such information. This is not feasible with today's quantum chemical software and computer facilities.

Iogansen proposed [59] an empiric relation between the bonding enthalpy, ΔH, of H-bonded complexes and the frequency shift of their OH stretch mode relative to that of the free molecule

$$\Delta H = 1.3(\Delta\nu)^{1/2}/\text{kJ mol}^{-1}\ \text{cm}^{-1/2} \quad (1)$$

where $\Delta\nu = \nu_{gas} - \nu_{complex}$.

With the monomeric MSA OH absorption at 3579.4 cm^{-1} (Table 1) and the 1:1 $MSA \cdot H_2O$ complex OH stretch mode assigned at 2930.0 cm^{-1}, the Iogansen relation indicates a complexation enthalpy of $\Delta H = -33.1$ kJ mol^{-1}, which compares very well with the theoretically calculated value.

Durig et al. [14] found two stable MSA dimeric complexes of symmetry C_i and C_{2h}, respectively. Our calculations confirm the C_i-minimum energy structure, but the proposed C_{2h}-structure relaxes into a minimum of C_2-symmetry, illustrated in Fig. 5 along with the C_i-structure which is the lower energy conformer by only 2.4 kJ mol^{-1}. The enthalpy change and Gibbs free energy upon complex formation of the C_i-dimer is calculated as −66.8 and −15.8 kJ mol^{-1}, respectively, at 298.15 K, Table 5.

With the OH stretch band of the MSA dimer of C_i symmetry at 3030.0 cm^{-1} (Table 3), the Iogansen relation yields a dimerization enthalpy of $\Delta H = -30.5$ kJ mol^{-1} per bond which, again, compares well with the above ab initio calculation.

6. Summary

Vapor species of methanesulfonic acid (MSA, CH_3SO_2OH) trapped in solid Ar and Ar/H_2O matrices were

investigated by FTIR spectroscopy. Intensity changes induced by matrix temperature cycling of annealing and recooling and variations in water content indicate band assignments to monomeric and dimeric MSA species and to the 1:1 $MSA \cdot H_2O$ complex. These assignments are discussed in relation to MP2 and DFT calculations employing the B3LYP functional using Dunning's correlation consistent aug-cc-pVTZ basis set with a simple scaling procedure applied to the vibrational frequencies. A single structure is suggested for the monomer. Two structures of slightly different stabilization energies with C_2 and C_i symmetries are suggested for the dimer. The bands of energetically more stable C_i dimer are predominant but evidence of the second structure is seen in the SO_2 stretch region. For the 1:1 $MSA \cdot H_2O$ complex, again, two stable structures could be calculated, but the observed bands can be interpreted in terms of one of these only.

In the series of related matrix isolated molecules, dimethyl sulfoxide ($(CH_3)_2SO_2$), methanesulfonic acid (CH_3SO_2OH) and sulfuric acid (H_2SO_4) the 1:1 complex with H_2O has been identified [16,17,30, this work]. However, for the latter, the red shifted ν(OH) band of the H-bonded hydroxyl group of the acid could not be located. The clear observation of this band in the present case and for HNO_3 [55,56], an acid of similar strength, makes this issue of the 'missing band' even more interesting.

References

[1] H. Berresheim, F.L. Eisele, J. Geophys. Res. 103 (1998) 1619.
[2] H. Berresheim, F.L. Eisele, D.J. Tanner, J.W. Huey, R.P. Thorn, A. Jefferson, J. Geophys. Res. 103 (1998) 1629.
[3] D. Davis, G. Chen, P. Kasibhatla, A. Jefferson, D. Tanner, F. Eisele, D. Lenschow, W. Neff, H. Berresheim, J. Geophys. Res. 103 (1998) 1657.
[4] I. Barnes, K.H. Becker, I. Patroescu, Atmos. Environ. 30 (1996) 1805.
[5] A. Jefferson, D.J. Tanner, F.L. Eisele, J.W. Huey, J. Crawford, D.D. Davis, G. Chen, A. Torres, H. Berresheim, J. Geophys. Res. 103 (1998) 1647.
[6] A.J. Hynes, P. Wine, D.H. Semmes, J. Phys. Chem. 90 (1986) 414.
[7] H. Berresheim, P. Wine, D. Davis, in: H. Singh (Ed.), Sulfur in the Atmosphere, Van Nostrand Reinhold, New York, 1995, pp. 251–307.
[8] S. Koga, H. Tanaka, J. Atmos. Chem. 17 (1993) 201.
[9] P. Davidovits, J.T. Jayne, S.X. Duan, D.R. Worsnop, M.S. Zahniser, C.E. Kolb, J. Phys. Chem. 95 (1991) 6337.
[10] N. Furukawa, H. Fujihara, The Chemistry of Sulphones and Sulphoxides, Wiley, New York, 1988.
[11] N. Mihalopulos, I. Barnes, K.H. Becker, Atmos. Environ. 26A (1992) 807.
[12] R.J. Gillespie, E.A. Robinson, Can. J. Chem. 40 (1962) 644.
[13] S.M. Chakalackal, F.E. Stafford, J. Am. Chem. Soc. 88 (1966) 4815.
[14] J.R. Durig, L. Zhou, T. Schwartz, T. Gounev, J. Raman Spectrosc. 31 (2000) 193.
[15] H.C. Allen, E.A. Raymond, G.L. Richmond, J. Phys. Chem. A 105 (2001) 1649.
[16] A. Givan, L.A. Larsen, A. Loewenschuss, C.J. Nielsen, J. Chem. Soc. Faraday Trans. 94 (1998) 827.
[17] A. Givan, L.A. Larsen, A. Loewenschuss, C.J. Nielsen, J. Mol. Struct. 509 (1999) 35.
[18] A. Givan, L.A. Larsen, A. Loewenschuss, C.J. Nielsen, J. Chem. Soc. Faraday Trans. 94 (1998) 2277.
[19] A. Givan, A. Loewenschuss, C.J. Nielsen, Phys. Chem. Chem. Phys. 1 (1999) 37.
[20] A. Givan, A. Loewenschuss, C.J. Nielsen, J. Phys. Chem. A 104 (2000) 3441.
[21] A. Givan, A. Loewenschuss, C.J. Nielsen, J. Mol. Struct. 604 (2002) 147.
[22] P. Beichert, O. Schrems, J. Phys. Chem. A 102 (1998) 10540.
[23] H. Arstila, K. Laaksonen, A. Laaksonen, J. Chem. Phys. 108 (1998) 1031.
[24] S. Re, Y. Osamura, K. Mookuma, J. Phys. Chem. A 103 (1999) 3535.
[25] A.R. Bandy, J.C. Ianni, J. Phys. Chem. A 102 (1998) 6533.
[26] C.J. Ding, K. Laasonen, A. Laaksonen, J. Phys. Chem. A 107 (2003) 8648.
[27] D.L. Fiacco, S.W. Hunt, K.R. Leopold, J. Am. Chem. Soc. 124 (2002) 4504.
[28] A.B. Horn, K.J. Sully, Phys. Chem. Chem. Phys. 1 (1999) 3801.
[29] K.L. Nash, K.J. Sully, A.B. Horn, J. Phys. Chem. 105 (2001) 9422.
[30] A. Givan, H. Grothe, A. Loewenschuss, C.J. Nielsen, Phys. Chem. Chem. Phys. 4 (2002) 255.
[31] N. Tang, H.R. Munkelwitz, J. Colloid Interface Sci. 141 (1991) 109.
[32] A.D. Becke, J. Chem. Phys. 98 (1993) 5648.
[33] M.J. Frisch, G.W. Trucks, H.B. Schlegel, G.E. Scuseria, M.A. Robb, J.R. Cheeseman, J.A. Montgomery, Jr., T. Vreven, K.N. Kudin, J.C. Burant, J.M. Millam, S.S. Iyengar, J. Tomasi, V. Barone, B. Mennucci, M. Cossi, G. Scalmani, N. Rega, G.A. Petersson, H. Nakatsuji, M. Hada, M. Ehara, K. Toyota, R. Fukuda, J. Hasegawa, M. Ishida, T. Nakajima, Y. Honda, O. Kitao, H. Nakai, M. Klene, X. Li, J.E. Knox, H.P. Hratchian, J.B. Cross, C. Adamo, J. Jaramillo, R. Gomperts, R.E. Stratmann, O. Yazyev, A.J. Austin, R. Cammi, C. Pomelli, J.W. Ochterski, P.Y. Ayala, K. Morokuma, G.A. Voth, P. Salvador, J.J. Dannenberg, V.G. Zakrzewski, S. Dapprich, A.D. Daniels, M.C. Strain, O. Farkas, D.K. Malick, A.D. Rabuck, K. Raghavachari, J.B. Foresman, J.V. Ortiz, Q. Cui, A.G. Baboul, S. Clifford, J. Cioslowski, B.B. Stefanov, G. Liu, A. Liashenko, P. Piskorz, I. Komaromi, R.L. Martin, D.J. Fox, T. Keith, M.A. Al-Laham, C.Y. Peng, A. Nanayakkara, M. Challacombe, P.M.W. Gill, B. Johnson, W. Chen, M.W. Wong, C. Gonzalez, J.A. Pople, GAUSSIAN 03W, Version 6.0, Gaussian, Inc., Pittsburgh, PA, 2003.
[34] T.H. Dunning Jr., J. Chem. Phys. 90 (1989) 1007.
[35] R.A. Kendall, T.H. Dunning Jr., R.J. Harrison, J. Chem. Phys. 96 (1992) 6796.
[36] D.E. Woon, T.H. Dunning Jr., J. Chem. Phys. 98 (1993) 1358.
[37] F.B. Van Duijneveldt, J.G.C.M. Van Duijneveldt-van de Rijdt, J.H. Van Lenthe, Chem. Rev. 94 (1994) 1873.
[38] D. Maillard, M. Allavena, J.P. Perchard, Spectrochim. Acta A 31 (1975) 1523.
[39] E. Catalano, D.E. Milligan, J. Chem. Phys. 30 (1959) 45.
[40] J.A. Glasel, J. Chem. Phys. 33 (1959) 252.
[41] R.L. Redington, D.E. Milligan, J. Chem. Phys. 37 (1962) 2161.
[42] R.L. Redington, D.E. Milligan, J. Chem. Phys. 39 (1963) 1276.
[43] A.J. Tursi, E.R. Nixon, J. Chem. Phys. 1970; 52.
[44] P.A. Kollman, A.D. Buckingham, Mol. Phys. 21 (1971) 567.
[45] G.P. Ayers, A.D.E. Pullin, Chem. Phys. Lett. 29 (1974) 609.
[46] G.P. Ayers, A.D.E. Pullin, Spectrochim. Acta A 32 (1976) 1629.
[47] G.P. Ayers, A.D.E. Pullin, Spectrochim. Acta A 32 (1976) 1641.
[48] G.P. Ayers, A.D.E. Pullin, Spectrochim. Acta A 32 (1976) 1689.
[49] G.P. Ayers, A.D.E. Pullin, Spectrochim. Acta A 32 (1976) 1695.
[50] L. Fredin, B. Nelander, G. Ribbegard, J. Chem. Phys. 66 (1977) 4065.
[51] L. Fredin, B. Nelander, G. Ribbegard, J. Chem. Phys. 66 (1977) 4073.
[52] R.M. Bentwood, A.J. Barnes, W.J. Orville-Thomas, Mol. Spectrosc. 84 (1980) 391.
[53] A. Engdahl, B. Nelander, J. Chem. Phys. 86 (1987) 4831.
[54] X. Michaut, A.M. Vasserot, L. Abouaf-Marguin, Vib. Spectrosc. 2004; 34.
[55] A.J. Barnes, E. Lasson, C.J. Nielsen, J. Mol. Struct. 322 (1994) 165.
[56] A.J. Barnes, E. Lasson, C.J. Nielsen, J. Chem. Soc. Faraday Trans. 91 (1995) 3111.
[57] P.R. McCurdy, W.P. Hess, S.S. Sotiris, J. Phys. Chem. A 106 (2002) 7628.
[58] H.G. Kjaergaard, J. Phys. Chem. 106 (2002) 2979.
[59] V. Iogansen, in: N.D. Sokolov (Ed.), Hydrogen Bonding, Nauka, Moscow, 1981 (in Russian).